Theor Chem Acc (2010) 125:621–635
DOI 10.1007/s00214-009-0682-1

REGULAR ARTICLE

Forces mediating protein–protein interactions: a computational study of p53 "approaching" MDM2

Shubhra Ghosh Dastidar · Arumugam Madhumalar · Gloria Fuentes · David P. Lane · Chandra S. Verma

Received: 15 September 2009 / Accepted: 31 October 2009 / Published online: 22 November 2009

Abstract The protein MDM2 forms a complex with the tumor suppressing protein p53 and targets it for proteolysis in order to down-regulate p53 in normal cells. Inhibition of this interaction is of therapeutic importance. Molecular dynamics simulations of the association between p53 and MDM2 have revealed mutual modulation of the two surfaces. Analysis of the simulations of the two species approaching each other in solution shows how long range electrostatics steers these two proteins together. The net electrostatics is controlled largely by a few cationic residues that surround the MDM2 binding site. There is an overall separation in electrostatics of MDM2 and p53 that are mutually complementary and drive association. Upon close approach, there is significant energetic strain as the charges are occluded from water (desolvated). However, the complexation is driven by packing interactions that lead to highly favorable van der Waals interactions. Although the complementarity of the electrostatics of the two surfaces is essential for the two partners to form a complex, steric collisions of Y100 and short ranged van der Waals interactions of F19, W23, L26 of p53 determine the final steps of native complex formation. The electrostatics seem to be evolutionarily conserved, including variations in both partners.

Keywords Molecular dynamics · Electrostatics · p53 · MDM2 · Protein–protein interaction

1 Introduction

The ubiquitin ligase MDM2 controls the levels of the tumor suppressor protein p53 in normal cells [1, 2]. In stressed cells (e.g. those suffering from DNA damage) phosphorylation is known to destabilize the complex between the N-terminus of MDM2 and the N-terminus of p53. This stabilizes p53 which then activates arrest, repair or apoptosis in these cells [2]. The discovery of tumours with highly upregulated MDM2 has lead to several studies aimed at developing peptides/small inhibitors that can displace p53 from MDM2 [3–7]. Structural data on apo and complexed forms of MDM2 show wide structural heterogeneity (RCSB codes: 1Z1M, 1YCR, 1RV1, 2GV2, 1T4F, 2Z5T, 2AXI), revealing a highly plastic binding pocket of MDM2 (see the movie in the supporting information file M1.ppt). Indeed computational studies have further revealed the extent of this complexity in modulating peptide binding and, supported by experimental evidence, have shown that one of the residues that lines the binding site, Y100, has a major role in modulating this plasticity [8, 9]. This immediately leads to the following questions: at what point does the conformational adjustment take place—is it a part of the binding event (induced fit) or does it occur prior to binding (pre-organized/lock-and-key)? What are the factors that control this modulation? It is known that long range steering [10] couples with short range effects (such as desolvation;

Dedicated to Professor Sandor Suhai on the occasion of his 65th birthday and published as part of the Suhai Festschrift Issue.

Electronic supplementary material The online version of this article (doi:10.1007/s00214-009-0682-1) contains supplementary material, which is available to authorized users.

S. G. Dastidar · A. Madhumalar · G. Fuentes · C. S. Verma (✉)
Bioinformatics Institute (A*STAR), 30 Biopolis Street, #07-01 Matrix, Singapore 138671, Singapore
e-mail: chandra@bii.a-star.edu.sg

D. P. Lane
p53 Laboratory (A*STAR), 8A Biomedical Grove, #06-06 Immunos, Singapore 138648, Singapore

ion-pair formation) and associated rearrangements to maximize intermolecular packing and are the hallmark of protein–protein interactions [11, 12]. Early studies demonstrated that it was possible using computational models to show how long range electrostatic steering forces could account for important biological phenomena such as the asymmetric polymerizations in actin [13]. Such studies paved the way for routine applications of these types of methods in exploring such phenomena, in particular those involving interactions between molecules such as proteins or proteins and nucleic acids [14]. These computational approaches have further been augmented by the representations of proteins as all atom models and as coarse grained models [15, 16]. A recent study has shown that in the p53–MDM2 system, conformational changes occur as p53 and MDM2 approach each other, such as the Y100 reorientations [17]. This study has revealed some of the conformational changes associated with the transition of MDM2 from uncomplexed (apo) to the complexed state, yielding a diversity of conformations. In addition, our own work has shown how the orientations of Y100 modulate the binding of p53 in different conformations [9, 18]. These simulations have revealed a rich complexity of interacting surfaces of p53 and MDM2. The interconversion between conformational states of MDM2 may be correlated to the binding of p53, yielding eventually the native structure of the complex. The probability of successful complexation between p53 and MDM2 is dependent on the dynamics of the conformations of both partners.

Based on available structural data and computational studies [8, 9, 19], we can classify the conformational states of MDM2 into the following three broad groups (see Fig. 1): (i) 'open' state, where the Y100 side chain points away from the p53 binding pocket; (ii) 'closed' state, where the Y100 side chain points towards the binding pocket resulting in some occlusion of the pocket and (iii) 'apo' state—the unliganded state of MDM2, where the Y100 is deeply buried and the p53 binding pocket is hardly accessible to a ligand. The 'open' state includes the crystal structure of the N-terminal domain of MDM2 complexed with a 13 residue fragment of the trans-activation domain of p53 (RCSB code 1YCR). The 'closed' state is revealed in the complex of MDM2 with the small molecule inhibitor nutlin (RCSB code 1RV1) and also several other peptide–MDM2 complexes. The 'apo' state is observed in the ensemble of NMR determined structures of MDM2 (1Z1M; [19]). Transitions between the 'open' and 'closed' states can occur during the process of mutual modulation of MDM2 and ligand as they writhe to optimize their interactions with each other, which has been seen in recent computational studies [9, 20].

Normally, a study of the diffusion of two molecules towards each other would best be carried out using the coarse grained method of Brownian dynamics (BD) simulations [21–23] (especially when they are charged overall; MDM2 has a net charge of +5e while the p53 fragment considered here has a net charge of −2e). Elcock et al. reported protein–protein association rates, calculated from BD simulations, which closely reproduced the experimentally observed kinetics; as well they suggested the role of electrostatics and the effect of ionic strength was underscored [24]. But in BD simulations proteins are treated as rigid bodies, i.e. conformational changes are not considered. However, it is clear from our earlier studies [9, 18] and those of others [17] that dynamics of individual side chains and conformational changes contribute significantly to the process under investigation. It is also known that at some stage these electrostatic attractions between MDM2 and p53 must switch to an interaction dominated by van der Waals forces, since eventually these are the forces that leads to a stable complex (see Supporting information in the references for the components of the binding free energy [9, 25]). Hence, for our purpose, analysis of atomistically detailed molecular dynamics is essential. Further, the exposed binding surface of uncomplexed MDM2 is highly hydrophobic in nature, and demands an explicit treatment of water molecules for accuracy [26], although recent progress in BD simulation in implicit solvent mode to study such processes seems promising [27]. For this reason, we examined in full atomic detail, the interactions between p53 and MDM2, under the influence of explicit treatment of waters and now attempt to extract the underlying noncovalent forces.

In this study, we have considered different sets of starting conditions each defined by placing the p53 at different distances from the MDM2 surface. For example, the native structure of the complex was taken and p53 was translated away from the MDM2 surface along the joining vector of the centre of masses of the MDM2 and p53 (using 'coor trans' command in CHARMM [28]). The magnitude of the translation characterizes the distance of separation between MDM2 and p53 in the starting structures (e.g. of 3 Å, 6 Å etc.) and has been summarized in Table 1. The crystal structure of the MDM2–p53 complex has the MDM2 in an 'open' conformation; to examine the other conformations of MDM2 (e.g. 'closed' and 'apo' states), the MDM2 structures with these different conformations were superimposed onto the crystallographic structure. These were then subject to MD simulations in explicit water. During the simulations we observed that MDM2 and p53 approached each other resulting in close encounters together with mutual modulations. The details of the structural changes along the trajectory have been reported elsewhere [18]. From these trajectories, representative snapshots were extracted and the role of electrostatics on complex formation has been analyzed.

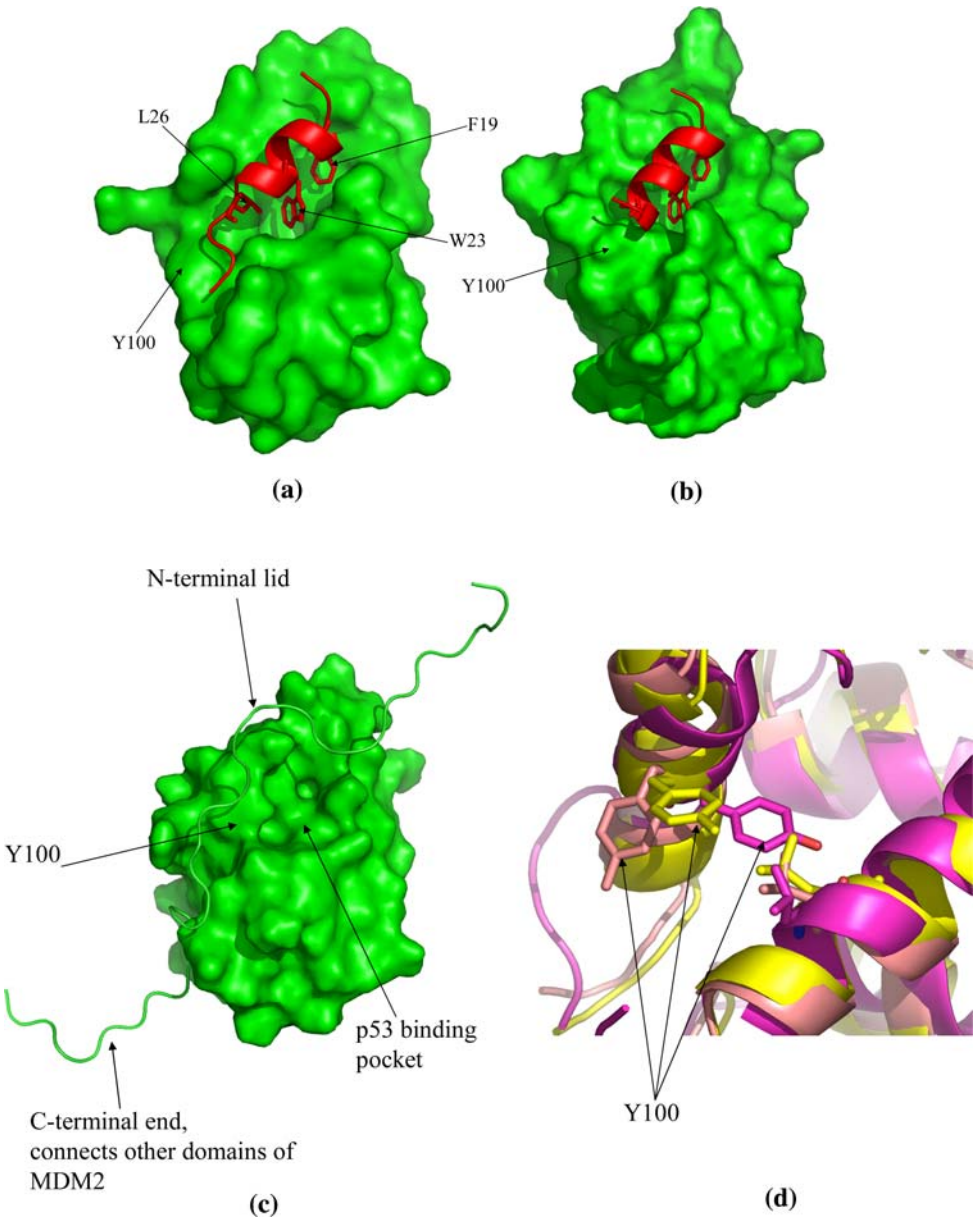

Fig. 1 Three different conformations of MDM2, classified according to the shape of the binding pocket (see text). **a** 'Open' conformation that binds the wild type p53 having the unstructured C-terminus. **b** 'Closed' conformation that gives a 'cozier' fit to an α-helical ligand. **c** The unliganded (apo) state of MDM2 where the binding pocked is relatively less accessible to the solvent. The NMR determined 'apo' state provides the structure of the N-terminal flexible lid structure that covers the binding pocket in absence of a ligand. The location of the Y100 has been pointed for each structure whose orientation primarily determines the shape of the binding pocket. **d** Superimposed structures **a–c** showing the difference of orientation of Y100: 'open' (*salmon red*), 'closed' (*yellow*) and 'apo (*purple*)

2 Methods

The crystal structure of the MDM2–p53 complex, consisting of residues 25–109 of MDM2 and 17–29 of p53 was the starting conformation of the 'open' state (RCSB entry 1YCR, resolved at 2.6 Å) [29]; the 'closed' state of MDM2 (residues 25–109) was obtained from our previous work [9] and the 'apo' state was obtained from the NMR ensemble (RCSB entry 1Z1M) [19]. The NMR structures have additional residues, both in the N-terminus (residues 1–24) and in the C-terminus (residues 110–119), which are absent in the crystal structure (resolved only residues 25–109). The starting structures of simulations were prepared by varying the distance of separation between MDM2 and p53 as described in previous section. The N-terminal region of MDM2, also referred to as its 'lid', consists of residues 1–24 (this region has three anionic residues). It is known to interact with the p53-binding cleft of MDM2 [30]. To study the interaction of p53 with the MDM2 binding pocket, we did not include the lid region in the simulations, while for the interactions between the lid and the MDM2 binding pocket we excluded p53 in those simulations. There is no evidence of the C-terminal region interacting with the p53-binding region and hence we exclude this region for any analysis. The protonation states of the titrable groups were set to mimic neutral pH, i.e., lysine and arginine side chains were kept at a charge of +1e each, while glutamic and aspartic acid side chains were maintained at a charge of −1e each. Molecular dynamics (MD) simulations in explicit water (TIP3P) [31] (using periodic boundary

Table 1 List of trajectories

	Trajectory name	MDM2 conformation	Translation of p53 in the starting structure (Å)	Length of the trajectory (ns)
1	Mo3A	Open	3	10
2	Mo6A	Open	6	10
3	Mc3AT1	Closed	3	20
4	Mc3AT2	Closed	3	20
5	Mc6A	Closed	6	40
6	M1n4A	Apo, model 1	4	20
7	M1n6A	Apo, model 1	6	10
8	M2n119	Apo, model 2 (residue 1–119)	NIL	15
9	M4n119	Apo, model 4 (residue 1–119)	NIL	10

The structures were prepared by translating p53 away from the binding pocket of MDM2. The magnitude of the translations have also been listed. Please see the Sects. 1 and 2 for details of the protocols

conditions) were carried out using the CHARMM22 force field [32] and the trajectories have been summarized in Table 1. The PME algorithm [33] was used to calculate the long ranged interactions while the short ranged interactions were truncated at 12 Å. SHAKE [34] was applied to freeze the vibrations of the bonds involving hydrogen atoms, enabling a 2 fs integration time step. The system was heated to 300 K followed by equilibration at constant pressure and temperature (NPT conditions). The production run was carried out at constant temperature and volume (NVT conditions). During the post-processing of the trajectory, representative snapshots were extracted after removal of explicit water and counter-ions. The components of binding/interaction energy of MDM2 and p53 were calculated following the MM/GBSA protocol using the GBSW model of implicit solvation [35]. Surface electrostatics were calculated using APBS [36]. For these, atomic charges were taken from CHARMM [28] and the conditions employed included a 0.15 M salt concentration at 300 K. The dielectric for the protein and solvent was set at 2 and 80, respectively.

The homology models of MDM2 of mouse, dog and bat were modeled based on the crystal structure of their human homologue, 1YCR (sequence identities between each of them are 92, 98 and 95%, respectively), while the homology model of Zebra fish was modeled based on that of frog MDM2, taken from the crystal structure 1YCQ (resolved at 2.3 Å, [29], sequence identity 64%). Alignment of the p53 peptide sequences was generated by CLUSTALW [37]. Three dimensional structures of the models were constructed using MODELLER [38]. All the figures of the molecular structures were prepared using PYMOL [39]. The 3D plots were generated using Matlab (Mathworks Inc.).

3 Results and discussion

3.1 The MDM2–p53 complex

The crystallographically determined structure of the complex between MDM2 (residue 25–109) and a small fragment of p53 (residue 17–29) summarizes the essential features of the interaction between the two proteins [7, 25, 29]. As shown in Fig. 1a, the residues F19 to L25 of the transactivation domain (TA) of p53 form an α-helical segment, projecting the three hydrophobic side chains (F19, W23 and L26) on the same face of the helix. These residues get embedded in the hydrophobic binding pocket of MDM2. While these three residues primarily determine the stability of its complex with MDM2 [29, 40], clearly residues at other positions are also important, an example being Y100 that can enable non-crystallographically observed conformations of the peptide to bind with equal affinity (see Fig. 1b) [9, 17, 20, 41]. There is a region of MDM2, referred to as the 'lid' (residues 1–24), visible only in the NMR structure due to its highly dynamic nature that can easily occlude the binding pocket of MDM2 (see Fig. 1c) [19, 42]. However, this interaction is thought to be weak and p53 can easily displace it [30].

3.2 Electrostatics of the crystal structure of p53–MDM2

The 17–29 region of p53 ($_{17}$ETFSDLWKLLPEN$_{29}$) has a net −2e charge, leading to a strong anionic potential around it (see Fig. 2) particularly at the C-terminus. In contrast, MDM2 has a net charge of +5e and this is reflected in the potential being largely cationic (see Fig. 2). The electrostatic complementarity clearly shows why complex formation takes place. Figures 2 and 3 show that this cationicity originates largely in 5 residues that lie near the p53 binding site (K51, R65, K70, K94, R97) although this is tempered to some extent by E25, E52 and E69. p53 on the other hand is largely anionic, due to E17, D21 and E28 with K24 providing some cationicity. The MDM2 also has an N-terminal lid region (residue 1–24) that has total charge of −1e, contributed by D11. It is clear that the smaller net negative charge on the lid relative to that on the p53 peptide explains partly why p53 displaces the lid easily [30]. This also explains how, upon phosphorylation (or introduction of an additional 2 units of negative charge) on S17 of the lid, the interaction with MDM2 will be stronger relative to p53 and the latter will be displaced, thus

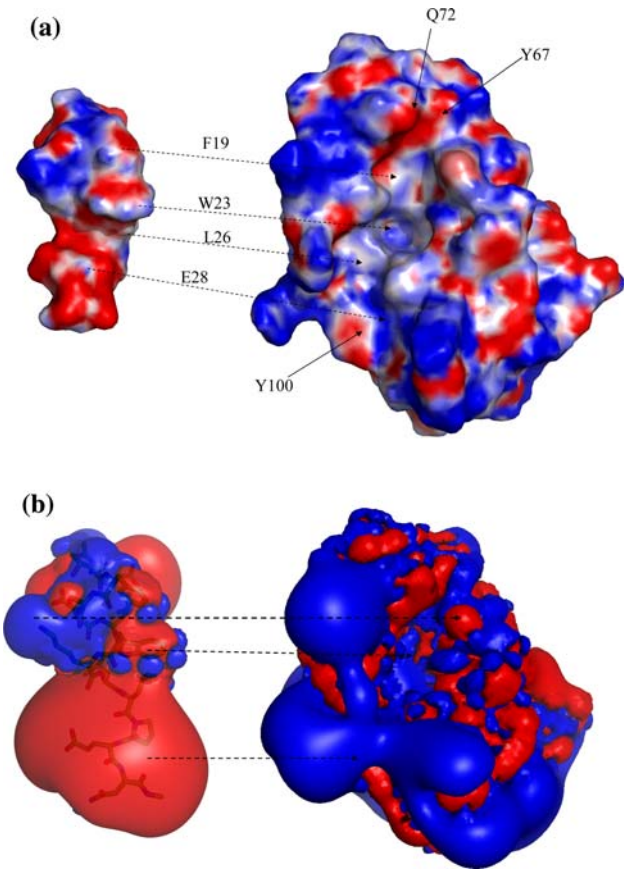

Fig. 2 **a** Surface electrostatics of MDM2 and p53 taken from their crystal structure (1YCR). The solid lined *arrows* point the location of key residues on the MDM2 surface whereas the *dashed arrows* point the contact regions of p53 residues on the MDM2 surface in the complexed state. The 'charge' complementarity of the contact regions are notable. **b** shows the isosurface of the same molecules. The color scale of electrostatics of the MDM2 surface is *red* (−5 kT/e) to blue (+5 kT/e). The contour level of the isosurface was set to ±1 kT/e. The same coloring scheme has been followed throughout the manuscript, in Figs. 3, 4, 5, 6, 7, 8, 9 and 13

stabilizing it against degradation—this is an important stress-related regulatory mechanism [43].

3.3 Open MDM2, p53 at 3 Å

When p53 is placed at 3 Å from MDM2 in its open state, i.e. with Y100 pointing away from the p53 binding site (see Fig. 1d), rapid complexation occurs leading to a conformation of p53 bound to MDM2 that is very close to the crystallographic complex (RMSD ∼1.7 Å). The overall electrostatics of MDM2 and p53 (see Fig. 4) are similar to the one characteristic of the crystallographic state. This shows a dipolar distribution across the binding region with the anionic region complementing the cationic end of p53 (the N-terminal end) and the cationic end dominating region of MDM2 complementing the anionic C-terminal half of p53 (see Fig. 2a); this distribution is quite robust to local fluctuations along the trajectory. Although the binding pocket is, by consensus, largely hydrophobic, it is clear that approach to this region is controlled by electrostatic effects that emanate from the cationic residues that surround the binding pocket. Studies have shown that W23 of p53 fits into the binding pocket of MDM2 and contributes to the stability in two ways: a large contribution from van der Waals interactions because of its larger size and W23 also forms an H-bond with the L54 backbone carbonyl [29]. It is interesting to note that the W23L mutation improves the electrostatic contribution to stability of the complex (data available in the supporting information of Ref. [9]). This partly arises because this mutation removes the partial positive charge on the side chain nitrogen of W23. Although this pocket is largely hydrophobic (as judged from the nature of the residues that line it), however, the influence of local partial charges on the protons of backbone nitrogens and the long range effects of the cationic residues impart the electrostatic potential in this region with a cationic character (this becomes apparent in the electrostatic maps when the charges on some of the side chains are switched off; see Fig. 3).

Within this largely cationic field of MDM2 that seems to steer p53, there are two regions of local anionicity (see Fig. 2). These two regions have been shown to be involved in modulating p53 binding [9, 20, 25, 37, 44]: one is localized at Y67/D68/E69 (near the binding site of the N-terminus of the p53 peptide) and the other at E25/Y100 (forms an H-bond with the C-terminus of the p53 peptide). It has been hypothesized that the former repels p53 when T18 is phosphorylated [25] thereby modulating its biological stability.

3.4 Closed MDM2, p53 at 3 Å

Next we retain the distance of p53 from MDM2 at 3 Å but use the conformation of MDM2 which has the Y100 pointing in towards the p53 binding region—the closed conformation. This results in a state where p53 is bound, but in two somewhat different conformations represented by trajectory Mc3AT1 and trajectory Mc3AT2 (see Fig. 5). In Mc3AT1, Y100 remains pointing inwards but L26 is never embedded completely. In contrast, in Mc3AT2, L26 does embed in, but now Y100 points outward creating space for L26. The other key residues in p53, F19 and W23 anchor into the right (native) location (see Fig. 5). But the orientations of Y100 only marginally affect the overall electrostatic potentials of the MDM2 surface. This occurs as a result of the reorientation of the hydroxyl group of the Y100 side chain. This is also observed in the nature of the isosurface (see Fig. 5), where most of the regions resemble the native complex (see for example Fig. 2). Indeed, the variations of the surfaces over the simulations clearly show

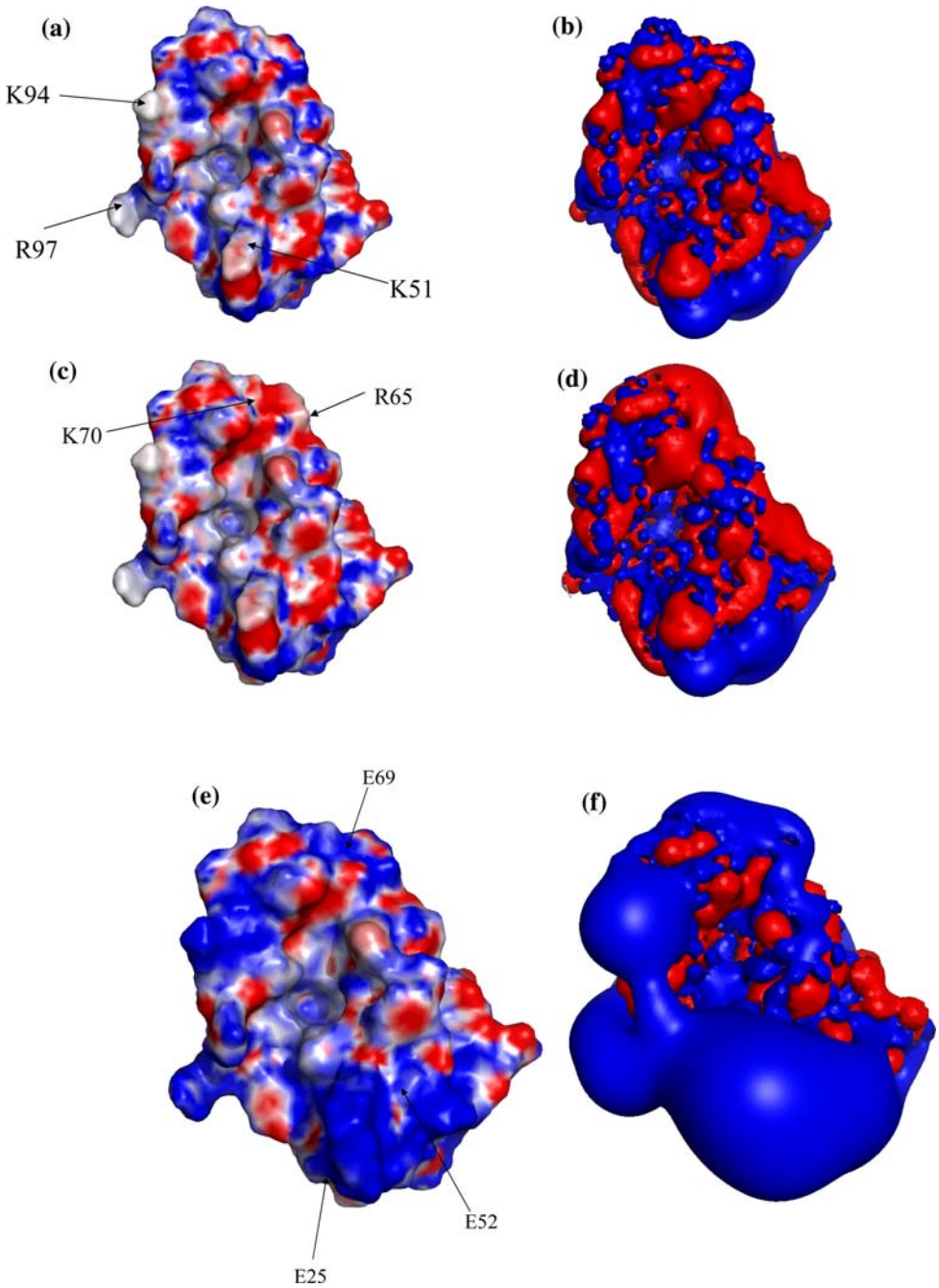

Fig. 3 **a** and **b** show the electrostatics after setting the side chain charges of K51, K94 and R97 to 'zero'; **c** and **d** show the electrostatics after setting the side chain charges of K51, R65, K70, K94 and R97 to 'zero'; **e** and **f** the same after setting the side chain charges of E25, E52 and E69 to 'zero'. Color coding as in Fig. 2

that the overall distribution is conserved. The structural variations of p53 (stabilized at ~3–5 Å relative to its "native" conformation) really arise from differences at its termini. It appears that while the overall diffusion of MDM2 and p53 is similar in either case, upon binding, the fine tuning is modulated by the orientation of Y100.

3.5 Open/closed MDM2, p53 at 6 Å

We next place p53 at a somewhat larger distance of ~6 Å with MDM2 in the 'closed' state. Within 2 ns (trajectory Mc6A), F19 and W23 of p53 get anchored in the binding pocket of MDM2 (see Movies in Ref. [18]). The initial steering that enables this encounter complex to form originates in the electrostatics of native-like MDM2 which funnels the peptide into the binding pocket. However, the "closed" state of MDM2 precludes the native conformation of the complex and results in the p53 peptide lying at an angle that is at ~15–20° from the direction of the native complex (Fig. 6), with an RMSD of ~8–10 Å from the wild type orientation. The closed conformations of Y100 preclude the L26 from entering, further aided by reorientations of M50 and L54 which further occlude the binding pocket. This results in F19 inserting into a hydrophobic

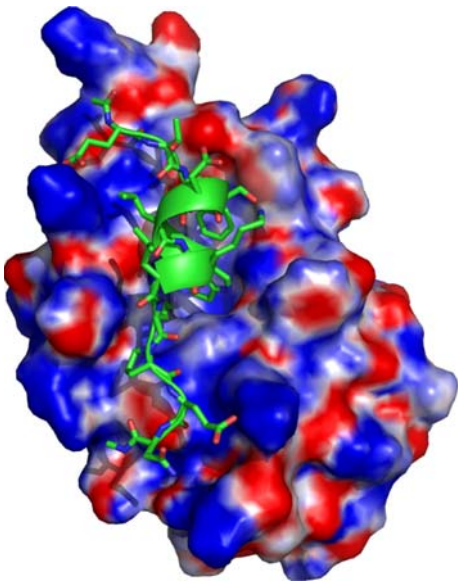

Fig. 4 Snapshot taken at the end of 10 ns MD of Mo3A (Table 1) trajectory that reproduces the native structure of the complex. Color coding as in Fig. 2

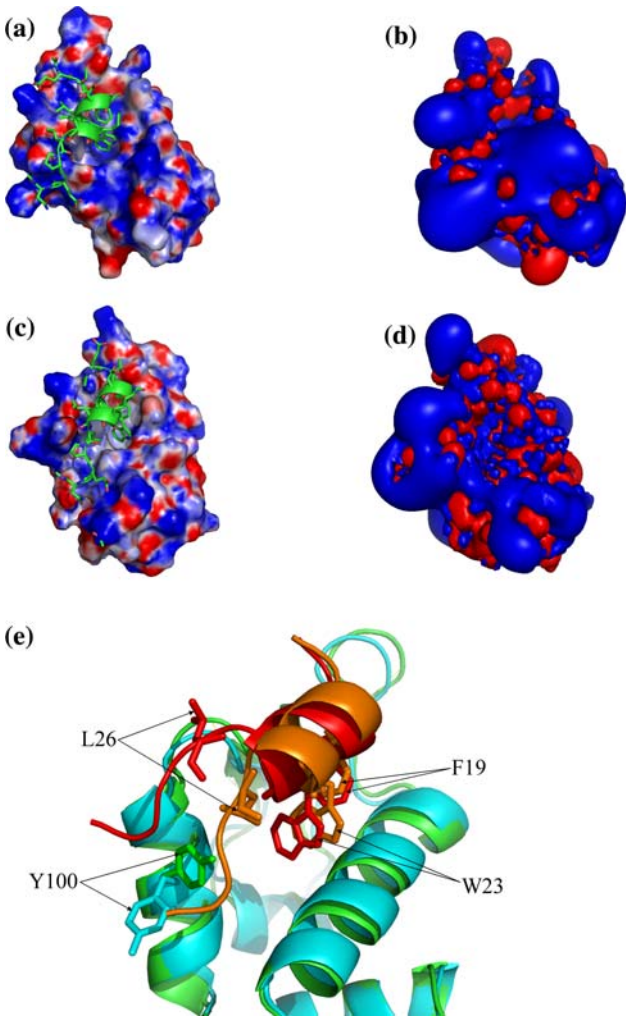

Fig. 5 **a** and **b** Electrostatic picture of the snapshot taken at the end of the trajectory of Mc3AT1 and **c** and **d** at the end of Mc3AT2 trajectory. **e** Superimposed snapshots show that the correlation between Y100 orientation and anchoring of L26 into binding pocket. *Green*-MDM2 and *red*-p53 correspond to Mc3AT1, *Cyan*-MDM2 and *orange*-p53 correspond to Mc3AT2. Color coding as in Fig. 2

pocket formed by L54, L57 and Y100 while W23 stabilizes against F55. This occurs by 12 ns and the peptide remains stable in this orientation (see Fig. 6 also see Movies in the supporting information of Ref. [18]). The major changes in the electrostatic fields are really only seen at the N-terminal end where local conformational changes bring R65 and E69 into salt bridging distance ($\sim$4Å). While the overall electrostatic landscape of MDM2 is conserved, the alternate orientation of p53 results in reduced electrostatics and van der Waals interactions (see Table 2).

When the starting conformation of MDM2 is "open" with the p53 initially located 6 Å away, the MDM2 immediately (within $\sim$1 ns) reverts to the "closed" state.

3.6 Apo state without lid, p53 at 4 Å

We next take a structure from the ensemble of NMR structures and place p53 at $\sim$4 Å. In this state, the side-chain of Y100 is buried inwards (see Figs. 1 and 7). At the end of 20 ns, the F19 and W23 residues of p53 embed into the binding pocket of MDM2 but residue L26 remains exposed on the surface (see Fig. 7). It was clear from our previous work [18] that Y100 remains stubbornly embedded in the binding site and occludes the binding pocket of L26. Comparison with the electrostatics of MDM2 after successful complexation (see Figs. 4, 5) shows that while there is reorganization of the electrostatic surface, the overall polarity is conserved. K51, K94 and R97 together provide the electrostatic force for (also see movie in supporting information) the C-terminal anionic end of p53 but the fact that L26 cannot embed leads to a different orientation of the C-terminal end of p53 relative to that seen in Fig. 1a.

3.7 Apo MDM2: role of the N-terminal lid region

The lid of MDM2 has been hypothesized to behave like a pseudo-substrate for the p53 binding pocket of MDM2 [42]; how the lid actually regulates the binding of p53 through phosphorylation is still unresolved [30]. We examine two distinct conformations of the lid that we take from the ensemble of NMR structures, one conformation consists of the lid in close contact with the binding surface and the second conformation consists of the lid pointing away from the surface. These two conformations represent the 'closed' and 'open' states of the lid and are model numbers 2 and 4, respectively of the NMR ensemble [19].

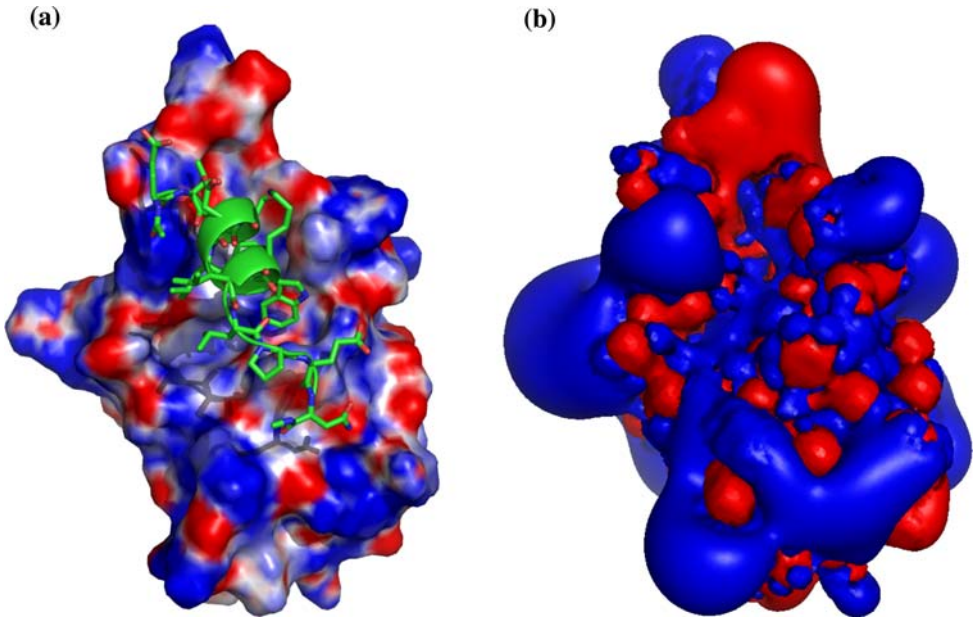

Fig. 6 Electrostatic picture of the snapshot taken at the end of Mc6A trajectory. **a** Molecular surface electrostatics with showing the bound p53 and **b** isosurface, p53 has not been shown. Color coding as in Fig. 2

Table 2 Change of components of molecular mechanical energy upon binding ($\Delta_{binding}$)

$\Delta_{binding}$	Native	Mo3A	Mc3AT1	Mc3AT2	Mo6A	Mc6A	M1n4A
$E_{electrostatic}$	−202.3	−353.0	−309.6	−277.1	−172.6	−182.0	−121.0
$E_{vanderWaals}$	−68.9	−59.7	−65.2	−55.2	−57.9	−44.7	−39.5
$E_{internal}$	7.6	7.3	4.3	13.9	8.5	9.6	11.0
E_{GB}	212.5	352.4	319.1	278.2	187.8	184.2	139.4
$E_{elec+GB}$	10.2	−0.6	9.5	1.1	15.2	2.2	18.4
$E_{solv(nonpolar)}$	−3.4	−3.4	−3.5	−3.3	−2.5	−2.2	−0.5
E_{total}	−54.5	−56.4	−54.9	−43.5	−36.7	−35.1	−10.6

For each trajectory only the change of the values with respect to the values of the uncomplexed states have been shown. The energy values are in kcal/mol. Data for 'Native' was available from our earlier work [9]

Comparison of the electrostatic surfaces of the two states shows that although there is some difference in the overall distribution of the potentials, the polarity is conserved (see Figs. 1, 8). Indeed the closed and open states of MDM2 with lid are characterized by 'in' and 'out' conformations of Y100, respectively, which controls the access to the binding site—a localized event as we have seen in our earlier studies [18].

3.8 Binding of MDMX

MDMX also binds p53 through a domain that is highly homologous to the N-terminal domain of MDM2 [45]. Crystallographically determined structures show high similarity of binding mode with p53 to MDM2 (PDB code 3DAB) [46]. However, in contrast to the net charge of +5e in MDM2, MDMX has only a net charge of +1e (MDM2 has an excess of 3 Lysines and 1 Arginine). As expected, p53 shows lower affinity for binding to MDMX than it does with MDM2 [47]. However, the overall distributions of the electrostatic potentials are similar between MDM2 and MDMX (see Fig. 9). Like in MDM2, the negatively charged side chains, E17 and E28 of p53 occupy regions of MDMX that have cationic character.

3.9 Energetics

Computational studies have shown that the MDM2–p53 complex is driven by van der Waals forces [9, 20, 25, 48]. In the native complex, the gain in electrostatic energy cannot compensate for the loss of solvation energy and thus destabilizes binding by ∼10 kcal/mol (see Table 2). However, this is offset significantly by the stabilizing van der Waals energy (∼69 kcal/mol). In the various trajectories, we find a strong correlation between the ability to dock into the native-like state and the underlying energetics (see Table 2). It is clear from all the simulations that charge–charge interactions stabilize the complexes but are offset by the penalty paid for burying the charges (sum of electrostatic (E_{elec}) and polar component of solvation

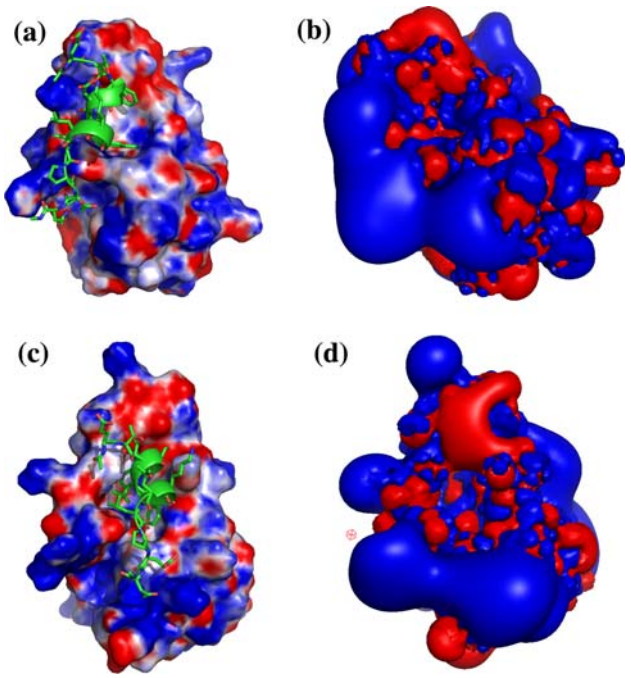

Fig. 7 **a** and **b** are different representations of a snapshot taken before the MD in the M1n4A trajectory; **c** and **d** are different representations of a snapshot taken at the end of this trajectory. The trajectory was generated from an unliganded, NMR-derived conformation of MDM2 with the p53 placed near the binding site

(E_{GB})). The net stabilization that drives complex formation in all cases originates in packing/van der Waals interactions. The high electrostatic interaction energies (Mo3A, Mc3AT1, Mc3AT2) are indicative of the orientation of p53 with respect to MDM2 resulting in favorable polar interactions. The somewhat lower (compared to native) van der Waals energy in Mo3A indicates poorer packing, but has the highest electrostatic stabilization and smaller desolvation penalty. Mc3AT1 is quite native-like, except for optimal packing of L26; the similarity of total energies suggests that the conformation with L26 pointing out may well be accessible amongst the space explored by the native complex (see Table 3).

We decided to carry out a simple investigation. For both MDM2 and MDMX, the p53 peptide was moved away from the surface of MDM2/MDMX and the complex and the energetics examined along the pathway (Figs. 10, 11). To do this, for each complex, the native structure was optimized using 1000 steps of adopted basis Newton–Raphson (ABNR) minimizer and then the ligand (p53) was translated along the vector that connects the centres of masses of MDM2/MDMX and p53, away from the MDM2/MDMX surface at $\sim$2 Å steps, until a separation of $\sim$50 Å. Each step of translation was followed by 300 steps of ABNR minimization and the snapshot was saved. The energy of binding/interactions between MDM2/MDMX and p53 was evaluated at each point (see Fig. 10) following

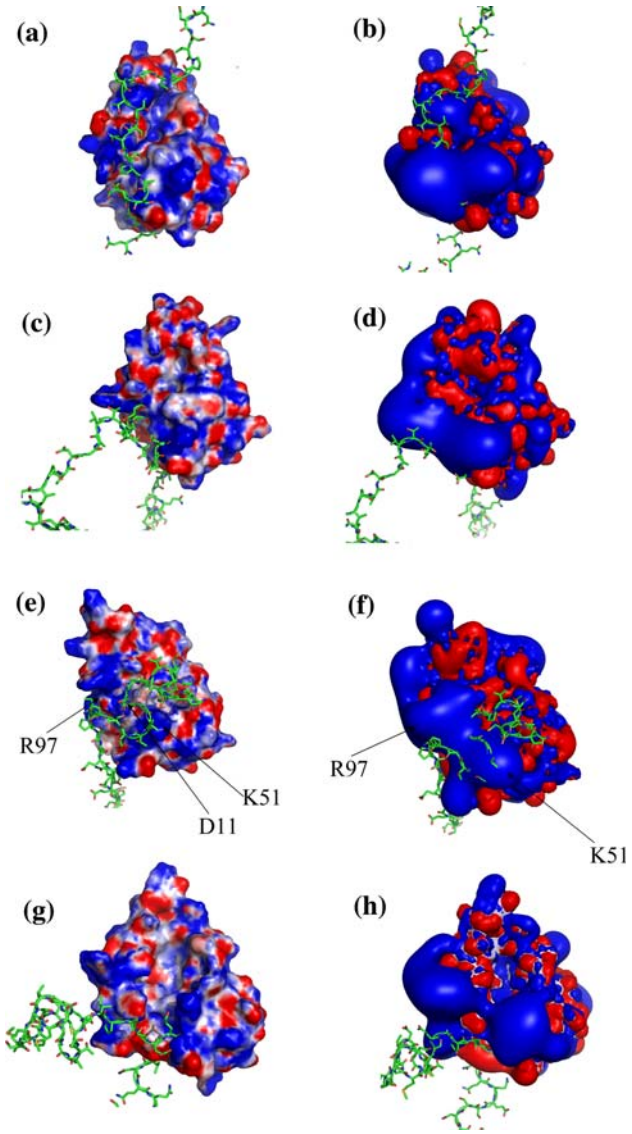

Fig. 8 Apo structures of MDM2 having the lid in **a**, **b**, **e** and **f** open and **c**, **d**, **g** and **h** closed situation. **a**–**d** are the electrostatics of the structures before MD simulation and **e**–**h** are the for the structure obtained at the end of MD simulation (trajectory M2n119 and M4n119 in Table 1)

the MM/GBSA protocol, applying the GBSW solvation model. It is clear that the electrostatics dominates in steering the two partners together; however, at close range, there is a switch and the penalty for bringing the charged residues into close proximity and excluded from solvent results in a large penalty making the net electrostatic contribution unfavorable. In parallel, the van der Waals switches to overwhelming stabilization. The quantitative profiles will no doubt depend upon the number of steps of minimization carried out. To examine this, we repeated this experiment, but with an initial 2000 ABNR step minimization followed by 600 steps of ABNR minimization after each step of translation. It is clear that the overall trend is

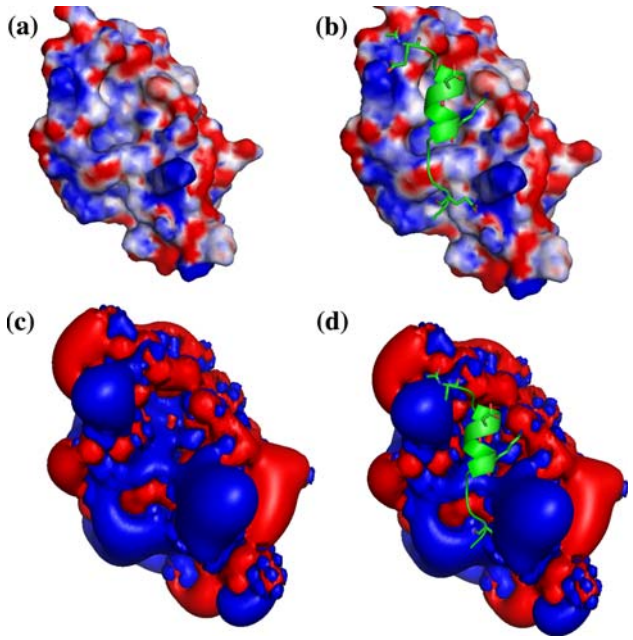

Fig. 9 Surface electrostatics and isosurface potentials of MDMX extracted from the crystal structure (PDB code 3DAB) bound to p53. For each representation the complexed state has been shown for easier identification of the binding pocket of the surface

Table 3 Description of the movie files

Movie file name	Description
Supplementary material 1	Modulation of the binding pocket of MDM2 to bind different ligands. MDM2 structures have been extracted from the PDBs (see the 'Introduction' in the main text) and then have been joined them as a movie. MDM2 is presented with molecular surface. The structures of the ligands have been shown
Supplementary material 2	The variation of the 'isosurface' of MDM2 along the trajectory 'Mc3AT1'
Supplementary material 3	The variation of the 'isosurface' of MDM2 along the trajectory 'Mc3AT2'
Supplementary material 4	The variation of the 'isosurface' of MDM2 along the trajectory 'Mc6A'
Supplementary material 5	The variation of the 'isosurface' of MDM2 along the trajectory 'M1n4A'
Supplementary material 6	The variation of the 'isosurface' of MDM2 along the trajectory 'Mo6A'

similar (dashed lines in Fig. 10a) although at larger separation there are some changes in the profiles and the overall curve is smoother. However, at closer separations the profiles are very similar. Again it is the overall trends that are important for our current study rather than the absolute quantities. We see this pattern for both MDM2 and MDMX and this pattern presumably will be characteristic of such interactions in general. Overall, the plots of interaction energies along the trajectories show that the van der Waals interactions are comparable for all the situations we have examined, varying between −50 and −70 kcal/mol. This is because although the location of p53 varies with respect to the native complex, nevertheless the peptide stays very close to the surface and makes packing interactions. However, the exact location of p53 relative to the surface will clearly lead to largely varying electrostatic energies, which is what we see in our calculations. Differing starting conformations lead to different binding modes, some of which are native-like and some not. In order to further extend this exploration, after each step of translation, the p53 peptide was rotated in the plane (orthogonal to the direction of translation) followed by 300 steps of minimization and computation of binding/interaction energy. The corresponding energetics (Fig. 11) show very nicely how the pattern of Fig. 10 is repeated and how indeed it is at closer range that most of the binding is driven by van der Waals interactions. Further, it is clear that at large separation, the peptide is driven by electrostatic attractions, with orientation not playing a significant role. However, as the peptide approaches MDM2, around 15 Å, the energetically optimal orientation of p53 is close to the bound state and a "funnel" appears that drives binding which is increasingly driven by van der Waals attractions. This switch in the nature of interactions is somehow reminiscent of a phase transition. We know that this reaction is exothermic [41] and this is a thermodynamic signature of a first order phase transition. Moreover, the dynamics show clearly that complexation does proceed with some nucleation—in this case some residues anchor each other across the interface between Mdm2 and p53 initially, following which the peptide is subsequently embedded completely. In order to examine the entropic components associated with these changes, we took six snapshots along the binding trajectory and computed the vibrational entropy of the complexes [49]. Although this is a simple approximation, nevertheless the results of this are in line with the structural–energetic changes outlined so far. The decrease in entropy (see Fig. 12) as p53 and MDM2 approach each other (to within 5 Å) can be understood by the fact that as the two separated molecules approach each other and influence each other, low frequency global modes with a higher entropic contribution appear. However, at close range, specific interactions start forming and hence getting more directed (due to the formation of electrostatic interactions and packing between p53 and MDM2) and hence motions start getting frozen. This reduces the low frequency modes of vibration, resulting in the observed decreases in entropy. A clear change in the density of states is not apparent as the origin of the entropic change is distributed across many different modes of vibration.

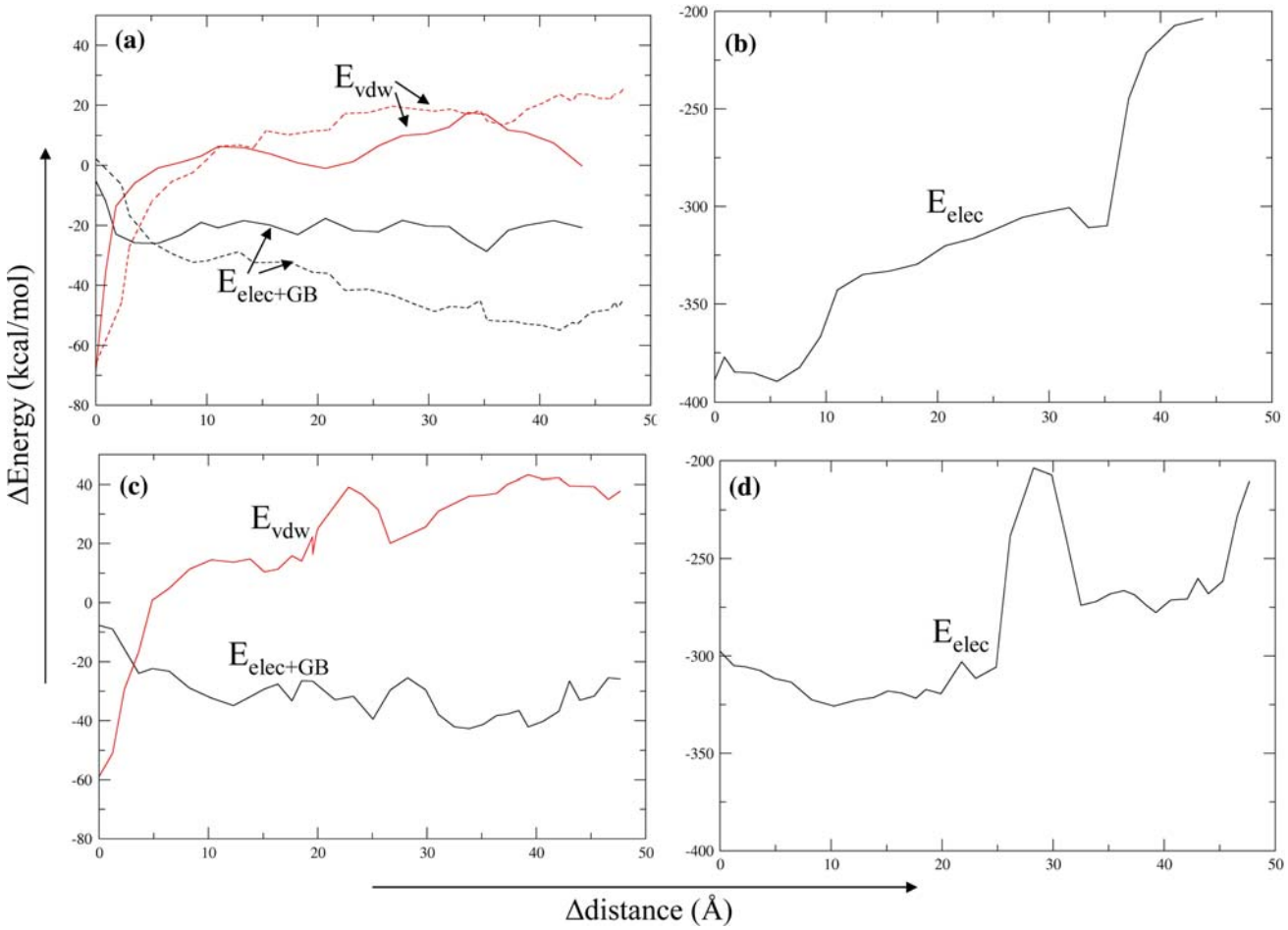

Fig. 10 Plot of different components of energies of interactions between MDM2/MDMX and p53, as a function of distance of separation between backbone 'O' atom of L54 of MDM2 (M53 for MDMX) and side chain 'N' atom of W23 of p53. **a** and **b** are for MDM2–p53 complex and **c** and **d** are for MDMX–p53 complex. The 'Δdistance' along the horizontal axis is the change of distance (defined above) with respect to the distances in their native complexes. The p53 was translated away (in ~2 Å step size) from the binding pocket of MDM2/MDMX starting from the native structure of the complex. At each point energy minimization was followed by calculations of the components of energy, using the GBSW implicit solvent model. $E_{\text{elec+GB}}$ is the sum of electrostatic component and GBSW solvation energy; E_{vdw} is the van der Waals component and E_{elec} is the electrostatic component. 'ΔEnergy' along the vertical axis represents the change of energy components upon complex formation, where the energy minimized uncomplexed MDM2/MDMX and p53 (extracted from the native structures of the complex) were considered as reference. The absolute values of ΔEnergy components are dependent on the choice of the reference state and the extent of energy minimization, which is also reflected in the non vanishing van der Waals interactions at the larger distances. The *dashed lines* in **a** indicates a repetition of the calculation with different number of steps of minimization (see text)

Despite the entropic reduction, complexation occurs due to enthalpic stabilization. A more detailed study of this process using dynamical models is currently under progress.

The distribution of key cationic residues (such as K51, R65, K70, K94, R97) must have evolutionary significance. MDMX lacks a positive charge at the equivalent position of R97 in MDM2 which is localized near the C-terminal end of the p53 peptide and this is partly responsible for the reduced affinity (manuscript in preparation). But overall the conservation of the electrostatic potential and the conservation of features seen in our simulations suggest a functional significance. The cationicity is conserved across species (see Fig. 13) and indeed we see this not only amongst the higher organisms (92–98% identity) but also with some variation, in other species too (60–70% identity); there are of course associated changes in p53 (see Fig. 14). In general, it appears that electrostatic steering brings the peptide to the surface after which packing interactions dominate. This can be followed by rapid sequestration of F19 and W23 but there is a larger variance in the orientation of L26 which in turn is correlated with that of Y100. While the peptide can "drift" over the surface of MDM2, the overall electrostatic field does act to constrain the peptide in a "funnel" and restrains it from drifting away (see movie

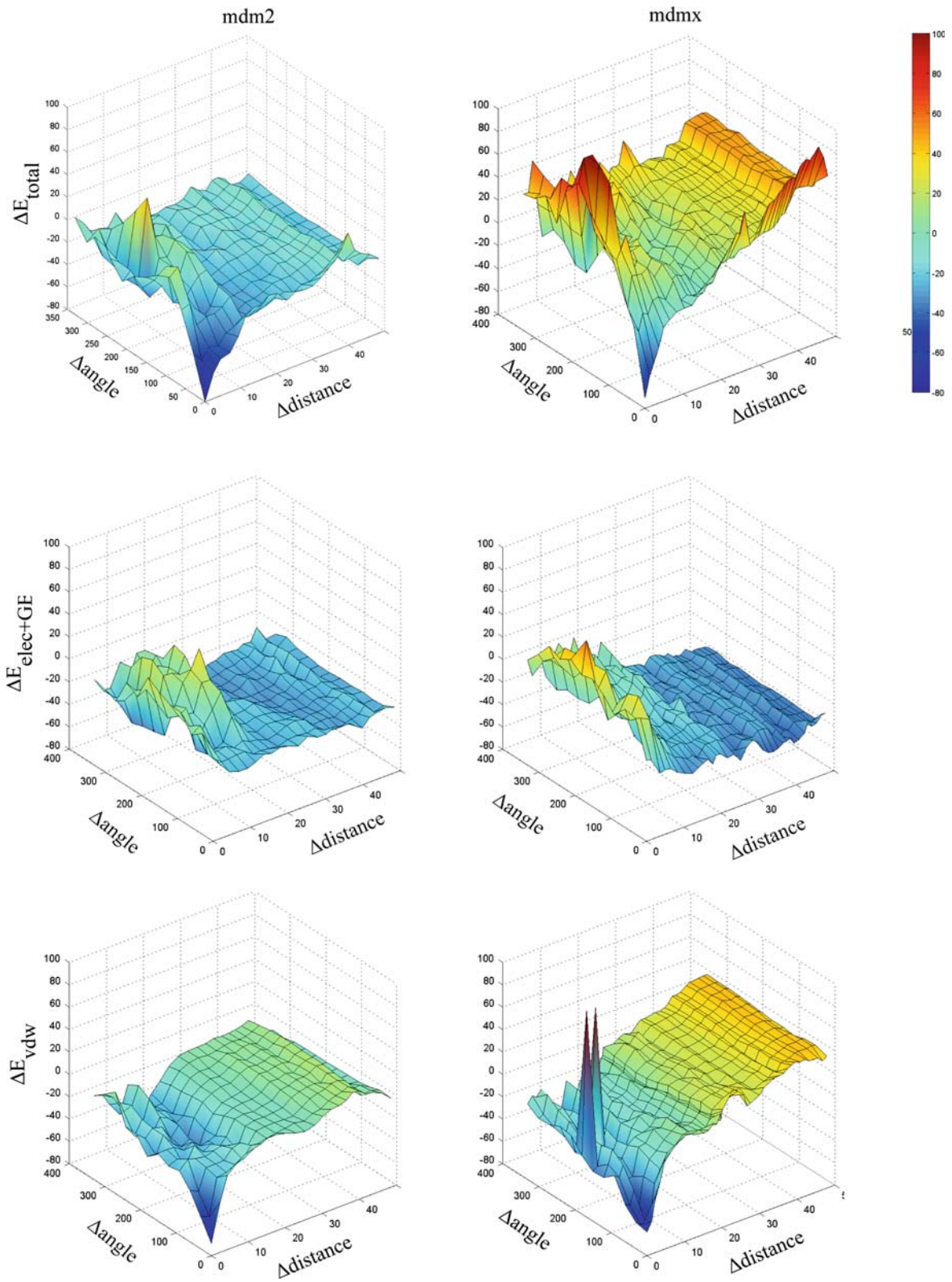

Fig. 11 Plot of different components of energies of interactions between MDM2/MDMX and p53 which has been explained in Fig. 10. In this plot at each distance of separation 'Δdistance' (in Å) p53 has been rotated with respect to the axis connecting the centre of masses of MDM2/MDMX and p53, with an increment of 30° (plotted along the axis 'Δangle' (in degree) and minimized energy was calculated at each step of rotation. The vertical axis shows the change of energy (in kcal/mol) upon complex formation (same as is Fig. 10)

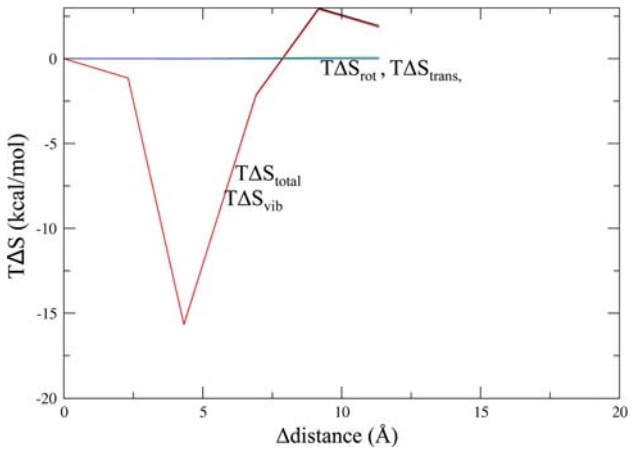

Fig. 12 Plot of variation entropy (ΔS) of complex formation as a function of distance of separation of between MDM2 and p53 (Δdistance, as defined in Figs. 10, 11), calculated from normal mode analysis. The absolute values of entropy of the MDM2–p53 system at each point have been subtracted from the entropy of the wild type complex. The ΔS has been multiplied with temperature ($T = 300$ K). The rotational (S_{rot}) and translational (S_{trans}) component of entropy remains almost unchanged (so two lines are superimposed) whereas the change in vibrational component determine the change in total entropy (S_{total})

M6_Mo6A.mpg). This is in accord with mechanisms proposed to underlie protein–protein interactions and protein–ligand interactions [10, 11, 50].

Our studies and the evolution of the two sequences suggest that electrostatics plays a significant role. However, this is in contrast to some reports that have found no evidence of salt dependence on the interactions of p53 with MDM2, thus suggesting a lack of significant electrostatic effects [41]. The issue is further complicated by reports in the same study that shortening the p53 peptide, including removal of one negative charge (E28), leads to a 2.5-fold increase in k_{on}. In all the trajectories reported here we find that the electrostatic interactions fall rapidly when complex formation occurs (mostly when near-native complexation occurs). The isosurface of the MDM2 conformations shows that the complementarity is maintained when p53 approaches the open state of MDM2. This map is perturbed if p53 is displaced into a non-native orientation. This builds upon our earlier demonstrations [9, 18] as well as our current findings, that the approach to, and eventual complex formation, are both highly dynamic processes and are characterized by extensive modulation of each others properties

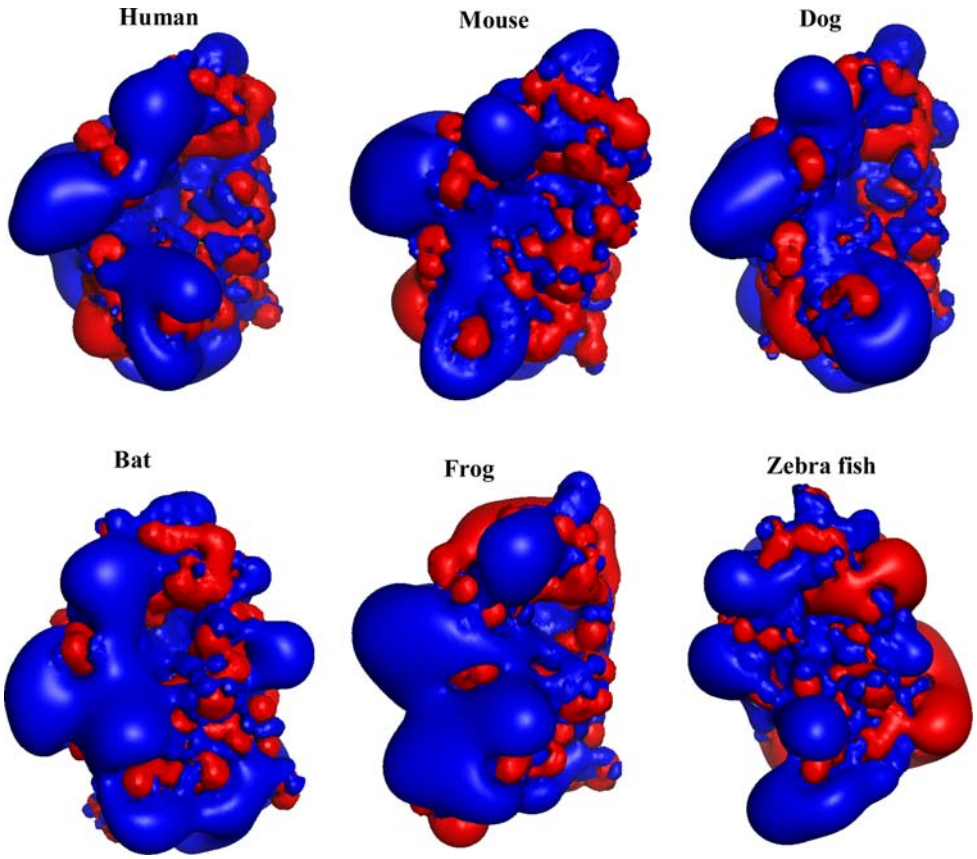

Fig. 13 Isosurface potentials of MDM2 of different species

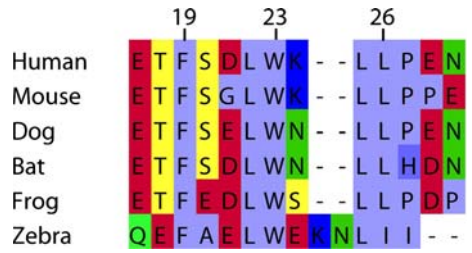

Fig. 14 The sequence alignment of residues of the fragment of p53 that corresponds to our study. The comparison has been done for the same set of species that is shown in Fig. 13

[9, 20]. Hence, it appears as no surprise that changes to the length of the peptides and/or mutations can indeed significantly influence the rates of approach of the two partners to each other.

4 Conclusions

Recent studies have shown that plasticity of MDM2 has a large influence in the ligand binding and the conformational changes at the MDM2-peptide interface and originates in the mutual modulation of ligand and receptor [9, 20]. This is also reflected in the diverse thermodynamic origins of complex stability [9]. In our previous work we have demonstrated that the plasticity of MDM2 and the binding of ligand is largely influenced by a few residues (primarily by Y100 [18]). It has been demonstrated that when p53 approaches the binding pocket of MDM2, the orientation of Y100 determines binding and thus it acts as a putative gate-keeper [18]. The orientation of Y100 is relevant when receptor and ligand are close enough to be influenced by the steric collision of side chains, but it may not influence the "approach" of p53 at larger separations. Our present study investigates the factors that influence the approach of p53 and this study reveals that long range electrostatics steer p53 and MDM2 towards each other leading to complex formation. We find how the affinity is modulated by strong electrostatic attractions that dominate the energy landscape at long range, while at close range the attraction undergoes a switch to being dominated by van der Waals interactions. Once the two proteins interact, the electrostatic interactions are strongly destabilized as the charges are occluded from solvent (desolvated). The packing interactions then drive eventual complex formation. At large distances, there is an entropic drive that steers the two molecules together while at short distances, as specific interactions form, they freeze out degrees of freedom, leading to entropic destabilization; the final complexation is driven enthalpically. Non-native conformations of MDM2 exert somewhat altered electrostatics that in turn correlate with mispacking of p53 on the MDM2 surface. However, the surface electrostatics are strong enough to restrain the mispacked p53 from drifting away and the residues which have been observed (from simulation) to have a role in such interactions, have also been found to be evolutionarily conserved. We are currently analyzing the role of such evolutionarily conserved residues in the 'approach and binding' of p53 and will be presented in a separate manuscript elsewhere.

Acknowledgments This work was supported by the Biomedical Research Council (Agency for Science, Technology and Research), Singapore. We thank Ivy Law of BII for technical help with Matlab.

References

1. Naski N et al (2009) Cell Cycle 8:31
2. Vogelstein B, Lane D, Levine AJ (2000) Nature 408:307
3. Bottger A et al (1997) Curr Biol 7:860
4. Moll UM, Petrenko O (2003) Mol Cancer Res 1:1001
5. Sakurai K, Schubert C, Kahne D (2006) J Am Chem Soc 128:11000
6. Vassilev LT et al (2004) Science 303:844
7. Zhong H, Carlson HA (2005) Proteins 58:222
8. Buolamwini JK, Addo J, Kamath S, Patil S, Mason D, Ores M (2005) Curr Cancer Drug Targets 5:57
9. Dastidar SG, Lane DP, Verma CS (2008) J Am Chem Soc 130:3514
10. McCammon JA (2009) Proc Natl Acad Sci USA 106:683
11. Blundell TL, Fernandez-Recio J (2006) Nature 444:279
12. Tang C, Iwahara J, Clore GM (2006) Nature 444:383
13. Sept D, Elcock AH, McCammon JA (1999) J Mol Biol 294:1181
14. Richter S, Wenzell A, Stein M, Gabdoulline RR, Wade RC (2008) Nucleic Acid Res 36:W276
15. Heath AP, Kavraki LE, Clementi C (2007) Proteins 68:646
16. Knotts TA, Rathore N, Schwartz DC, de Pablo JJ (2007) J Chem Phys 126:084901
17. Macchiarulo A, Giacche N, Carotti A, Baroni M, Cruciani G, Pellicciari R (2008) J Chem Inf Model 48:1999
18. Dastidar SG, Lane DP, Verma CS, BMC Bioinformatics (in press)
19. Uhrinova S, Uhrin D, Powers H, Watt K, Zheleva D, Fischer P, McInnes C, Barlow PN (2005) J Mol Biol 350:587
20. Madhumalar A, Lee HJ, Brown CJ, Lane DP, Verma C (2009) Cell Cycle 8:2828
21. Feldman-Salit A, Wirtz M, Hell R, Wade RC (2009) J Mol Biol 386:37
22. Gabdoulline RR, Wade RC (1998) Methods 14:329
23. Gabdoulline RR, Wade RC (2001) J Mol Biol 306:1139
24. Elcock AH, Gabdoulline RR, Wade RC, McCammon JA (1999) J Mol Biol 291:149
25. Lee HJ, Srinivasan D, Coomber D, Lane DP, Verma CS (2007) Cell Cycle 6:2604
26. Setny P, Geller M (2006) J Chem Phys 125:144717
27. Gabdoulline RR, Wade RC (2009) J Am Chem Soc 131:9230
28. Brooks BR et al (2009) J Comp Chem 30:1545
29. Kussie PH, Gorina S, Marechal V, Elenbaas B, Moreau J, Levine AJ, Pavletich NP (1996) Science 274:948
30. Worrall EG, Wawrzynow B, Worrall L, Walkinshaw M, Ball KL, Hupp TR (2009) J Chem Biol 2:113

31. Jorgensen WL, Chandrasekhar J, Madura JD, Impey RW, Klein ML (1983) J Chem Phys 79:926
32. MacKerell AD Jr et al (1998) J Phys Chem B 102:3586
33. Darden T, York D, Pedersen L (1993) J Chem Phys 98:10089
34. Ryckaert JP, Ciccotti G, Berendsen HTC (1977) J Comp Phys 23:327
35. Im W, Lee MS, Brooks CL 3rd (2003) J Comp Chem 24:1691
36. Baker NA, Sept D, Joseph S, Holst MJ, McCammon JA (2001) Proc Natl Acad Sci USA 98:10037
37. Thompson JD, Higgins DG, Gibson TJ (1994) Nucleic Acid Res 22:4673
38. Sali A, Blundell TL (1993) J Mol Biol 234:779
39. DeLano WL (2002) The Pymol molecular graphics system. DeLano Scientific, San Carlos
40. Bottger A, Bottger V, Garcia-Echeverria C, Chene P, Hochkeppel HK, Sampson W, Ang K, Howard SF, Picksley SM, Lane DP (1997) J Mol Biol 269:744
41. Schon O, Friedler A, Bycroft M, Freund SM, Fersht AR (2002) J Mol Biol 323:491
42. Showalter SA, Bruschweiler-Li L, Johnson E, Zhang F, Bruschweiler R (2008) J Am Chem Soc 130:6472
43. Shimizu H, Hupp TR (2003) Trends Biochem Sci 28:346
44. Freedman DA, Epstein CB, Roth JC, Levine AJ (1997) Mol Med 3:248
45. Czarna A, Popowicz GM, Pecak A, Wolf S, Dubin G, Holak TA (2009) Cell Cycle 8:1176
46. Popowicz GM, Czarna A, Holak TA (2008) Cell Cycle 7:2441
47. Hu B, Gilkes DM, Chen J (2007) Cancer Res 67:8810
48. Massova I, Kollman PA (1999) J Am Chem Soc 121:8133
49. Van Vlijmen HWT, Karplus M (1999) J Phys Chem B 10:3009
50. Jones S, Thornton JM (1996) Proc Natl Acad Sci USA 93:13